MODELLING OF PELLET-CLAD INTERACTION DURING POWER RAMPS

G. Zhou[1], J.E. Lindbäck[1], H.C. Schutte[2], L.O. Jernkvist[3], A.R. Massih[3,4]
[1]Westinghouse Electric Sweden AB, SE-72163 Västerås, Sweden
[2]Westinghouse Electric Company, 5801 Bluff Road, Columbia, SC 29209, USA
[3]Quantum Technologies AB, Uppsala Science Park, SE-75183 Uppsala, Sweden
[4]Malmö University, SE-20506 Malmö, Sweden

Abstract
A computational method to describe the pellet-clad interaction phenomenon is presented. The method accounts for the mechanical contact between fragmented pellets and the Zircaloy clad, as well as for chemical reaction of fission products with Zircaloy during power ramps. Possible pellet-clad contact states, soft, hard and friction, are taken into account in the computational algorithm. The clad is treated as an elastic-plastic-viscoplastic material with irradiation hardening. Iodine-induced stress corrosion cracking is described by using a fracture mechanics-based model for crack propagation. This integrated approach is used to evaluate two power ramp experiments made on boiling water reactor fuel rods in test reactors. The influence of the pellet-clad coefficient of friction on clad deformation is evaluated and discussed. Also, clad deformations, pellet-clad gap size and fission product gas release for one of the ramped rods are calculated and compared with measured data.

Introduction

Pellet-clad interaction (PCI) is one of the major issues in fuel rod design and reactor core operation in light water reactors (LWRs). PCI-induced clad tube failure is caused by a combination of stresses in the Zircaloy clad due to the pellet-clad contact pressure and chemical reaction of corrosive fission products, such as iodine released during operation, with Zircaloy under a power ramp. If the induced stresses in the clad are sufficiently large and the concentration of the fission product is amply high, clad failure may occur. PCI has been a topic of numerous experimental and computational studies with a great amount of accumulated field experience. This has lead to PCI-resistant designs and operation guidelines, which have dramatically reduced the propensity for such failures in recent years. Overviews, from industrial perspective, on PCI testing and computations relating to LWR fuels can be found in [1,2]. Cox has reviewed the PCI failure mechanism in [3]. Some recent analyses on both structural and fracture aspects of PCI are given in [4,5].

In this paper, we present a computational method to describe PCI. The pellet-clad contact model used accounts for friction and soft/hard contact due to fragmented (relocated) fuel pellets. The effect of the iodine-induced stress corrosion cracking is described by using a fracture mechanics-based model for crack propagation in line with ref. [6]. We evaluate two power ramp experiments made on boiling water reactor (BWR) fuel rods in test reactors; a power ramp test made on a fresh fuel pin in the Halden reactor some years ago; and a recent test made on a modern Westinghouse fuel pin, irradiated in a Swedish BWR and then ramped in the Studsvik R2 reactor.

The plan of this paper is as follows: First, we outline the principal PCI models used in our analysis. Next, the ramp tests under consideration are briefly described, followed by the results of our computations on these tests. Finally, we discuss the results of our computations in light of the experimental data.

The models

Mechanics

The pellet cladding mechanical interaction (PCMI) model used includes the effect of friction and axial mechanical interaction and associated rod elongation. The UO_2 fuel pellet is considered as rigid, but can deform by thermal expansion, densification and fission product swelling. The pellet radial (normal) displacement u_n^p is expressed as: $u_n^p = u_T + u_D + u_S$ where u_T, u_D, u_S are the radial pellet displacement due to thermal expansion, fuel densification and fuel swelling, respectively. Pellet fragments can also relocate during power rise. Pellet radial displacement due to relocation u_R is assumed to be a function of the radial contact pressure P_n defined as:

$$u_R\left(P_n\right) = \begin{cases} G_n^m\,(1 - P_n / P_n^m) & \text{if } 0 \le P_n \le P_n^m \\ 0 & \text{if } P_n^m < P_n \end{cases} \tag{1}$$

where G_n^m is the maximum pellet relocation, i.e. under zero contact pressure condition, and P_n^m is the minimum contact pressure to fully remove the relocation, $u_R = 0$ [7]. Pellet relocation in the axial direction is not considered.

A finite element (FE) method is used to calculate stresses and strains in the clad. The FE model assumes that the clad tube is an axisymmetric shell. The clad material is a zirconium alloy and it deforms by thermal expansion, elastic-plastic deformation and creep (viscoplastic deformation). The following assumptions are made in the mechanical model for the clad: (i) The clad tube is divided axially into a number of segments. (ii) Within each segment, stresses and strains are spatially constant. (iii) Within each segment, the axial displacement $v(r, z)$ is independent of radius r. (iv) Within each segment, the radial displacement $u(r, z)$ is independent of z.

The constitutive relation for Zircaloy clad that include thermoelasticity, plasticity, and creep is written as: $\boldsymbol{\sigma} = \boldsymbol{D}\,(\boldsymbol{\varepsilon}_m - d\boldsymbol{\varepsilon}_p)$, where $\boldsymbol{\varepsilon}_m = \boldsymbol{\varepsilon} - \boldsymbol{\varepsilon}_p + d\boldsymbol{\varepsilon}_p - \boldsymbol{\varepsilon}_c - \boldsymbol{\varepsilon}_T = \boldsymbol{\varepsilon}_e + d\boldsymbol{\varepsilon}_p$ is the modified elastic strain tensor and $\boldsymbol{\sigma}$ is the stress tensor. Here, $\boldsymbol{\varepsilon}$ is the total strain tensor, $\boldsymbol{\varepsilon}_p$ the total accumulated plastic strain, $d\boldsymbol{\varepsilon}_p$ the increment of plastic strain, $\boldsymbol{\varepsilon}_c$ include other strains (thermal, accumulated creep, irradiation growth), $\boldsymbol{\varepsilon}_T$, the thermoelastic strain, $\boldsymbol{\varepsilon}_e$ the elastic strain and $\boldsymbol{D}$ is the elasticity matrix. The yield stress σ_y of Zircaloy cladding is a function of strain, temperature and fast neutron fluence (≥1MeV). If yielding occurs, the plastic strain increment $d\boldsymbol{\varepsilon}_p$ is calculated through the Levy-Mises flow rule of associated plasticity. Isotropic hardening is assumed. For material properties of UO_2 and Zircaloy, we have employed the correlations given in [8], for Zircaloy creep [9] and pellet relocation [7].

The pellet-clad gap, defined as: $\boldsymbol{G} = \boldsymbol{G}^0 + \boldsymbol{u}^c + \boldsymbol{u}^p$, where, for each pellet-clad node-pair in the FE-model, $\boldsymbol{G} = (G_n, G_t)$ is the current gap size, $\boldsymbol{G}^0 = (G_n^0, G_t^0)$ the initial gap, $\boldsymbol{u}^p = (u_n^p, u_t^p)$ the pellet outer surface displacement, $\boldsymbol{u}^c = (u_n^c, u_t^c)$ the clad inner surface displacement; and the subscripts n and t denote the radial (normal) and the axial (tangential) gap components, respectively. G_n is the "relocated" gap, defined as $G_n = g_n + u_R$, where g_n is the non-relocated gap. Once G_n is known, g_n and P_n are computed according to the radial gap conditions tabulated below. Note that pellet relocation leads the to the states of soft and hard pellet-clad contact.

Radial gap conditions and states

G_n Condition	g_n Condition	P_n Condition	Gap State
$G_n = g_n + G_n^m \geq G_n^m$	$g_n = G_n - G_n^m \geq 0$	$P_n = 0$	Open
$0 \leq G_n \leq G_n^m$ $G_n = G_n^m(1 - P_n / P_n^m)$	$g_n = 0$	$0 \leq P_n \leq P_n^m$ $P_n = P_n^m(1 - G_n / G_n^m)$	Soft
$G_n = 0$	$g_n = 0$	$P_n^m \leq P_n$	Hard

Upon pellet-clad contact, the radial mechanical gap becomes zero and friction forces between the pellet and clad are generated. These friction forces (or stresses) are assumed to follow the Coulomb friction law, which describes the limiting friction needed to overcome prior to any sliding between the pellet and clad. Let P_t be the axial (tangential) friction contact stress and μ the friction coefficient, the friction contact conditions for $g_n = 0$ and $P_n > 0$ are:

$$|P_t| \leq \mu P_n; \qquad P_t = \mathrm{sgn}(\Delta G_t)\mu P_n, \tag{2}$$

where the first relation from the left designates the stick condition, while the second one the slip condition. Here, ΔG_t indicates the change in axial (tangential) gap G_t.

Fission product gas release

The fission product gas release process is modelled by assuming that UO_2 consists of spherical grains of equal size [10]. The fission product gases are produced at a rate $\beta(t)$ in a grain of radius $R(t)$. The gases migrate to grain boundaries by diffusion with a diffusion coefficient $D(t)$. The gas atoms reaching the boundary precipitate into intergranular bubbles with a local density of $N(t)$ (per unit area) and a grain boundary re-solution rate of $B(t)=b\lambda/2$, where b is the grain boundary re-solution frequency, and $\lambda/2$ the re-solution depth from the grain face. All these variables are assumed to be time-dependent. Gas atom concentration at position r at time t in the grain, $C(r,t)$, is described by:

$$\frac{\partial C(r,t)}{\partial t} = D(t)\nabla^2 C(r,t) + \beta(t) \quad \text{for} \quad 0 < r < R(t). \tag{3}$$

The imposed boundary conditions are $\partial C(0,t)/\partial r = 0$ and $C(R,t) = B(t)N(t)/D(t)$, with the initial condition $C(r,0)=0$. Gas diffusion and grain growth may occur simultaneously. Analytical solutions to the problem of gas diffusion in expanding medium have been used [11]. The intergranular gas density $N(t)$ is found to be:

$$N(t) = \frac{2}{3}R\int_0^t \beta(s)ds - \frac{2\int_0^R r^2 C(r,t)dr}{R^2}. \tag{4}$$

When the gas concentration at the grain boundary reaches a certain threshold level, given by $C_{\max}(t) = B(t)N_s(t)/D(t)$, gas release will occur. The gas atom density per unit area of grain boundary at saturation N_S is calculated through the ideal gas equation of state.

As can be noticed from Eq. (3), only the release of stable fission product gases (Xe and Kr) are calculated. Moreover, only the release of stable (long-lived) iodine isotopes is considered, and it is assumed to be proportional to the release of Xe [12].

Stress corrosion cracking

The combined effects of mechanical and chemical interaction with the fuel pellets may cause failure of the clad tube through stress corrosion cracking (SCC). This kind of failure is predicted with a model, in which the propagation of stress corrosion cracks is treated by use of linear elastic fracture mechanics (LEFM). The cracks are supposed to nucleate at pre-existing flaws at the clad inner surface, which are subjected to local stress concentrations induced by the opening of radial pellet cracks; see Fig. 1. The initial clad flaws are assumed to start growing transgranularly, provided that the stress intensity exceeds a critical threshold and that the clad material is chemically sensitised and thus susceptible to SCC; the latter condition is cast in the form of a threshold iodine concentration in the pellet-clad gap. The transgranular crack growth rate is in our model correlated to clad temperature T, stress intensity K_I, and iodine concentration C_I at the clad inner surface through [6]

$$\frac{\mathrm{d}a}{\mathrm{d}t} = F(C_I)\left(\frac{K_I}{K_{Iscc}}\right)^n e^{-Q/RT}. \tag{5}$$

Here, a is the crack length, F is a function of the iodine concentration, Q and n are constants, and K_{Iscc} is a material- and temperature-dependent threshold stress intensity for transgranular SCC. The incremental crack growth in each time step of an analysis is evaluated through Eq. (5) for each axial segment of the fuel rod. The stress intensity factor is estimated from the current crack length, pellet-clad contact pressure and clad average hoop stress through superposition of analytical solutions [12]

$$K_I = \frac{\tau R_i\theta}{\sqrt{\pi a}} f_1\left(\frac{R_i\theta}{2a}\right) f_2\left(\frac{a}{w}\right) + \sigma_{\theta\theta}\sqrt{\pi a}\; f_3\left(\frac{a}{w},\frac{R_i}{w}\right). \tag{6}$$

Here, f_1, f_2 and f_3 are dimension-free functions and R_i is the clad inner radius; other parameters are defined in Fig. 1. The first term on the right-hand-side of Eq. (6) accounts for the local effect of frictional shear forces ($\tau \equiv P_t = \mu P_n$) from the pellet, whereas the second term is related to the uniform loading in the hoop direction ($\sigma_{\theta\theta}$).

Ramp tests

We have used the aforementioned integrated models to evaluate some power ramp experiments made on BWR fuel rods in test reactors. In particular, we analyze a "classical" power ramp test that was made on fresh fuel pins, with a narrow pellet-clad gap, in the Halden reactor some years ago; and a recent test made on modern Westinghouse fuel, irradiated in a Swedish BWR, and then ramped in the Studsvik R2 reactor.

Halden IFA404 test

The first power ramp experiment evaluated in our paper is a PCMI test performed in the Halden reactor in Norway within the Instrumented Fuel Assembly, IFA-404 test series [13]. In particular, we consider the pin number 403 in the test IFA-404-1. The pin was an unirradiated BWR fuel rod with a rather small pellet-clad gap size. The technical data for this rod are presented in Table 1. One objective of this test was to measure the diameter increase and the length changes of the pin as a function of linear heat generation rate (LHGR) during power cycling. The power ramp was performed by increasing the LHGR of the pin from nearly zero to a peak value of around 50 kW/m. The power was kept at this level for nearly 24 h, and then slowly reduced. Fig. 2 displays the power history for this test. Both the elongation and the diameter profile of the rod were measured during the power cycling. The results in terms of the clad circumferential and axial strains versus LHGR, extracted pointwise from continuous measurements, are presented in Table 2.

Studsvik SVEA-96S test

The considered test was conducted on a Westinghouse 10×10 SVEA96-S fuel assembly rod, base irradiated in the Barsebäck 2 BWR in Sweden, 1999-2002, to a rod burnup of about 32 MWd/kgU, Fig. 3. A test pin of length 570 mm with UO_2 fuel pellets was disassembled from the original (segmented) rod for power ramp testing in the Studsvik R2 reactor. Basic technical data on the fuel pin are given in Table 1. The pin was non-destructively examined in hot cell at Studsvik. Examination covered pin diameter measurements and γ-spectrometry. The R2 test facility and experimental technique for fuel ramp test is described in [14]. For the considered test, a pressurised water loop was used for simulating BWR coolant conditions (9 MPa, 285°C). The rod surface temperature was limited by sub-cooled surface boiling, implying that the rod surface temperature may not exceed the saturation temperature (303°C) by more than a few degrees.

The pin was subjected to irradiation in R2 by first raising the power from zero to 12 kW/m very rapidly. This initial power step was followed by a slow power increase during a period of 25 minutes until the conditioning LHGR of 22.5 kW/m was reached. Conditioning means that a fuel pin reaches a state of thermo-mechanical equilibrium at a constant LHGR after a sufficient period of time; in this case about 12 h. After conditioning, the pin was subjected to a power ramp, where a ramp step height of around 5 kW/m and a step duration of 1 h were utilised. The step ramp rate is about 6.4 kW/m/min. The ramp terminal level (RTL) was about 56.5 kW/m. Power was held at RTL for about 15 h, then LHGR was finally reduced to 7 kW/m after 50 minutes, upon which the irradiation was terminated. The pin survived the ramp. Fig. 4 shows the power history during the ramp test.

After the ramp test, the pin underwent post-irradiation examination (PIE) in hot cell at Studsvik. The PIE included γ-spectrometry, pin diameter, pellet-clad gap size, fuel density and fission product gas release measurements. The γ-spectrometry was performed along the pin for determination of specific nuclides comprising ^{137}Cs and ^{134}Cs. The rod diameter measurements were made at 4 circumferential positions along the pin. The pellet-clad gap size of the pin was determined by compressing the rod transversally between two parallel flat edges and measuring the pin deformation as function of applied force during the load cycle. The measurements were corrected for the elastic deformation of the apparatus. Fission product gas release was determined by first puncturing the pin in the plenum region, then measuring the internal gas pressure and determining the free volume. The amounts of released Xe and Kr gases were determined by mass spectroscopy analysis from retrieved samples. The fraction of fission gas release was determined by dividing the measured amount with the calculated amount of the generated inventory of these gases. Optical inspection of the clad inner surface revealed a large number of ≈10 μm deep flaws, but no through-wall cracks.

Table 3 lists pellet-clad gap size measurements, including the data on clad outer diameter. Fig. 6 shows the profilometry data on clad diameter before and after ramp, and Fig. 7 displays the relocated gap size along the fuel. Fraction of fission gas (Xe, Kr) release measured after ramp amounted to 32%, with a corresponding rod internal pressure of 2.14 MPa at STP.

Computations

The models described in the foregoing sections are included in the fuel rod thermal-mechanical code STAV. We used this code to evaluate the Halden and the Studsvik ramp tests. The Halden IFA-404 test was performed on a fresh fuel pin, with virtually no fission gas release. Hence, it was purely a PCMI test. The results of the computations on hoop and axial strains are presented in Figs. 5a and 5b, respectively, together with some measured data, see also Table 2. Calculations were performed for $\mu =$ 0.0 and $\mu = 0.014$. From Fig. 5, it is seen that the results are satisfactory for $\mu = 0.014$. The peak clad hoop stress is calculated to be $\sigma_{\theta\theta} = 320$ MPa, while the corresponding pellet-clad contact pressure is P_n= 65 MPa. Our calculations show that SCC of the clad tube does not occur, since the amount of iodine in the pellet-clad gap is negligible. The calculated maximum stress intensity at an assumed, 10 μm deep, clad inner surface flaw was 2.3 MPam$^{1/2}$.

Computations for the Studsvik test were performed with $\mu = 0.014$. Results are presented in terms of calculated clad outer diameter before and after ramp, together with measured data in Fig. 6. Fig. 7 depicts the calculated relocated pellet-clad gap vs. measured values along the fuel. The peak hoop stress is calculated to be $\sigma_{\theta\theta} = 790$ MPa with the corresponding contact pressure $P_n = 123$ MPa. The yield strength in that location of the clad is calculated to be 679 MPa. Hence, some pure plastic deformation occurs, even for highly irradiation-hardened Zircaloy, under such a severe ramp. Our calculations show that the maximum stress intensity at the observed 10 µm deep flaws at the clad inner surface is 4.9 $\mathrm{MPam}^{1/2}$. The base irradiation fission gas release fraction is calculated to be around 0.3%, while the value after the ramp is calculated as 26.3%, which is below the measured value of 32%.

Discussion

The results of the calculations on the Halden pin show the strong effect of friction forces on the behaviour of axial clad deformations during PCMI; Fig. 5. Hence a proper modelling of the contact problem is essential for prediction of fuel deformation during strong PCMI. The friction coefficient used in our calculations ($\mu = 0.014$) is considered to be an effective (empirical) value that includes the influence of pellet relocation and cracking. It differs from the measured value of the dynamic friction coefficient, between UO_2 and Zircaloy, which is reported to be in the range 0.5-0.7 [15].

In the case of the Studsvik pin, we observe from Fig. 6 that the clad outer diameter is somewhat underestimated after the ramp. This is mainly attributed to the gaseous fuel swelling during power ramp, which is not taken into account in the present model. Neither have we modelled the thermal creep deformations of UO_2, which is expected to occur for $T > 0.5T_m$, with T_m being the melting temperature. The precise calculation of pellet-clad gap is more involved, since the pellets undergo complex cracking and distortion under the influence of temperature gradients during a ramp, Fig. 7. The calculated fission gas release fraction is underestimated by the gas atom diffusion model utilised here. At RTL of 56.6 kW/m, Fig. 4, the peak calculated fuel central temperature is 2530 K with the corresponding pellet surface temperature 767 K. Consequently, the fuel is subjected to a considerable temperature gradient at the ramp terminal power. This kind of temperature gradient can trigger other modes of fission gas migration in the fuel than the atomic diffusion considered in our calculations, e.g. gas bubble motion and bubble coalescence. Furthermore, the PCMI method utilised here is essentially a one-dimensional model, although the effect of axial forces on the clad is accounted for through a finite element method. Therefore, the occurrence of the pronounced clad ridging observed cannot be captured, Fig. 6. This requires a more detailed 2- and 3-dimensional modelling, which is beyond the intention of the fast 1-d fuel rod thermal-mechanical analysis code used here.

In the presented SCC failure model, transgranular crack growth is assumed to initiate at pre-existing internal flaws. This approach is based on the observation that surface defects, up to a depth of about 20 µm, do exist in commercial clad tubes. An alternative approach would be to model the process of crack initiation from an initially smooth surface, which for iodine-induced SCC in zirconium alloys entails chemical preconditioning and slow intergranular crack growth. Another simplification made in our failure model is that the pellet-clad contact pressure and the clad hoop stress are calculated without consideration of the increase in clad tube compliance as the crack grows through the tube wall. Moreover, according to the ASTM standard E399, LEFM is not applicable to cracks shorter than $2.5(K_{Iscc}/\sigma_y)^2$. For irradiated Zircaloy-2 at 630 K, σ_y is approximately 700 MPa and K_{Iscc} 2.3 $\mathrm{MPam}^{1/2}$. Hence, the shortest cracks for which LEFM is valid are in this case 25-30 µm. These limitations can be overcome by use of non-linear fracture mechanics in a finite element framework, as described in [6]. However, this approach is computationally arduous, and is not suitable for standard design analyses.

Our correlation for stress corrosion crack growth in Eq. (5) is based on results from tests performed on mono-tubes of Zircaloy, and therefore must be extended to treat fuel rods with liner cladding. However, it is interesting to note that the calculated maximum stress intensity at the observed 10 μm long clad flaws in the liner rod was 4.9 MPam$^{1/2}$. In a non-liner rod, this stress intensity would most likely have lead to propagation of the flaws and to penetration of the clad tube.

Acknowledgement
We wish to extend our thanks to K. Kitano and U. Engman at Studsvik Nuclear, Sweden, for valuable communications.

References

[1] M. Gärtner, G. Fischer, *J. Nucl. Mater.,* 149 (1987) 29-40.
[2] A.R. Massih, L.O. Jernkvist, T. Rajala, *Nucl. Eng. Des.*, 156 (1995) 383-39l.
[3] B. Cox, *J. Nucl. Mater.,* 172 (1990) 249-292.
[4] J. Brochard et al., *Trans. SMiRT 16*, paper # 1314, Washington D.C., August 2001.
[5] G. Rousselier, S. Leclercq, O. Diard, *Trans. SMiRT 17*, paper # C03-3, Prague, August 2003.
[6] L.O. Jernkvist, *Nucl. Eng. Des.*, 156 (1995) 393-399.
[7] K. Forsberg, A.R. Massih, IAEA Proceedings, IWGFPT/32, 293-301, IAEA, Vienna, 1989.
[8] D.L. Hagrman, G.A. Reyman, MATPRO 11 Handbook, USNRC, NUREG/CR-0497, 1979.
[9] M. Limbäck, T. Andersson, ASTM STP 1295, 448-468, ASTM, W. Conshohocken, PA, 1996.
[10] M.V. Speight, *Nucl. Sci. Eng*., 37 (1979) 180-185.
[11] K. Forsberg, A. R. Massih, *Trans. SMiRT 16*, paper # 1931,Washington D.C., August 2001.
[12] L.O. Jernkvist, Quantum Technologies report, TR04-004, 2004.
[13] E. Kolstad, EHPG Meeting, Geilo, Norway, Report HRP 190, 1975.
[14] M. Carlsson, U. Engman, Studsvik technical note, N(R)-99/063, 1999.
[15] V.M. Shchavelin et al., *Atomnaya Energiya*, 61(3) (1986) 175-178.

Table 1. Data on fuel pins subjected to ramp tests.

Case	Halden	IFA404-1	Studsvik	SVEA96-S
Fuel pellet			As-fabricated	After BI
Material		UO_2	UO_2	-
Diameter	mm	12.64	8.25	8.34*
Length	mm	15	10	NM
Density	kg/m^3	10400	10600	NM
U235 content	wt%	7	4.2	-
Cladding			with ZrSn liner	-
Material*		RXA Zircaloy-2	RXA Zircaloy-2	-
Outer diameter	mm	14.3	9.63	9.61
Wall thickness	mm	0.8	0.635	NM
Pin				
Fill gas		Helium	Helium	
Fill pressure	MPa	0.1	0.4	NM
Active length	mm	500	472	475.5
Plenum volume	mm^3	8700	1560	NM

RXA: re-crystallised-annealed; * Calculated mean; BI: base irradiation; NM: not measured

Table 2. Halden IFA404-1 cladding hoop and axial strains vs. peak linear heat generation rate (PLHGR).

PLHR	Hoop	Axial	PLHGR	Hoop	Axial
kW/m	%	%	kW/m	%	%
0	0	0	46.4	-	-
1.1	0	0	43.3	-	0.095
9.5	-	0.007	39. 6	0.295	-
19.0	-	0.035	36.9	0.3	0.083
24.3	0.1	-	31.7	-	0.072
29.5	-	0.068	28	-	-
38.6	-	0.115	19.5	-	-
48.5	-	0.15	11.6	-	0.063
51.7	0.435	0.158	1.1	0.2	-

Table 3. Pin dimensions measured at Studsvik after ramp.

Axial position from bottom	Relocated diametral gap	Compressed diametral gap	Clad OD
mm	μm	μm	mm
82	24	48	9.658
92	26	56	9.664
102	38	65	9.676
274.5	12	62	9.728
284.5	18	58	9.731
294.5	12	75	9.727
386	13	70	9.693
396	18	65	9.684
406	23	73	9.675

OD: outer diameter

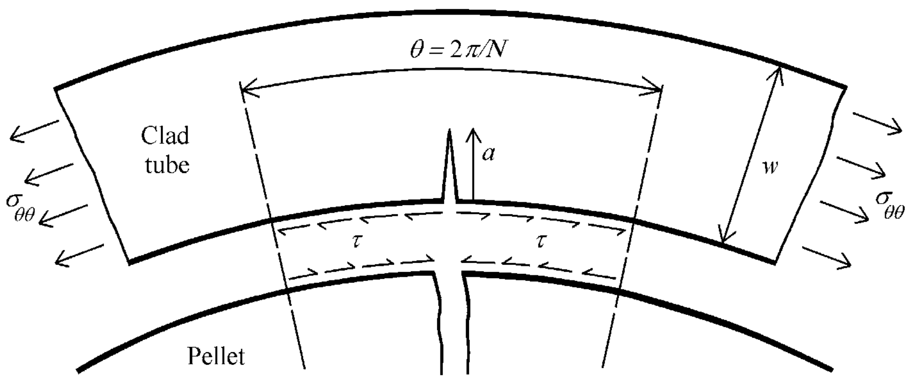

Figure 1. N symmetrically spaced radial pellets cracks are assumed. When the cracked fuel pellet expands, the cladding experiences local shear stresses from pellet-clad sliding, $\tau = \mu P_n$, where μ is the coefficient of pellet-clad friction, and P_n is the pellet-clad normal contact pressure.

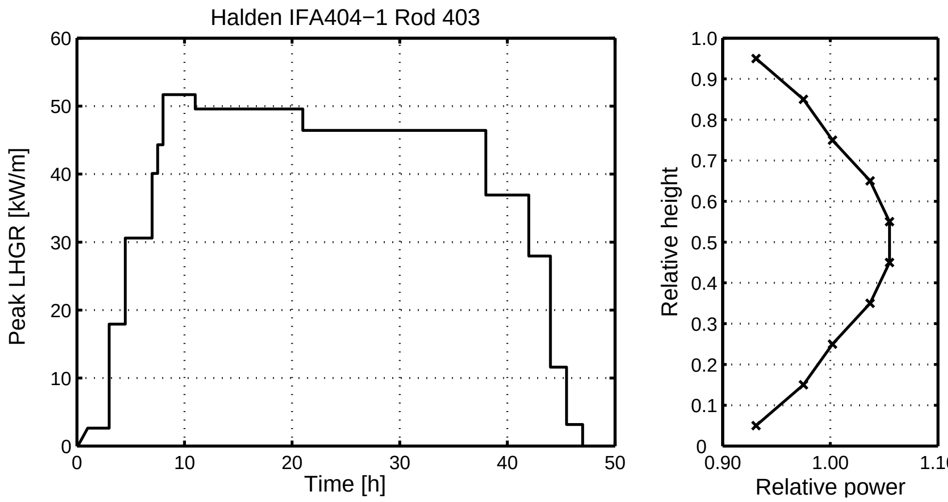

Figure 2. Power history and axial power profile along the fuel column for the Halden pin.

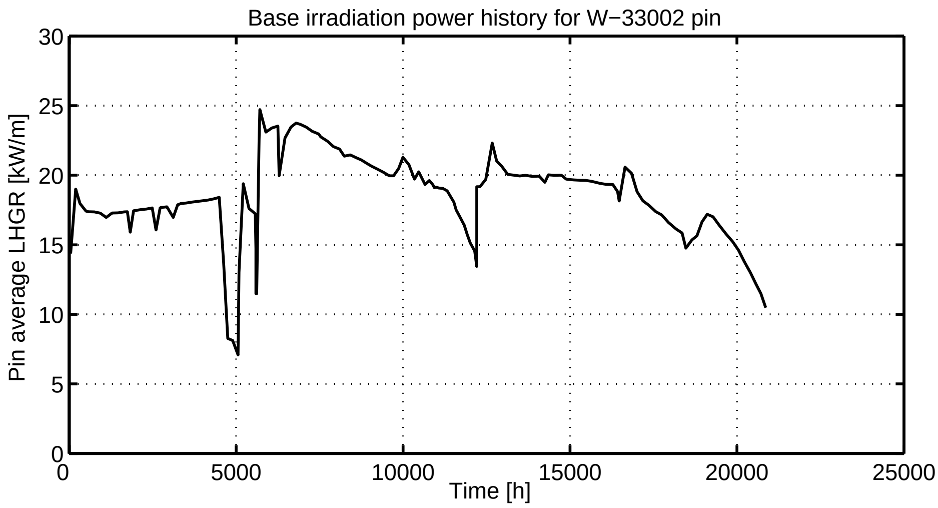

Figure 3. Base power history for the Studsvik pin, irradiated in the Barsebäck-2 BWR.

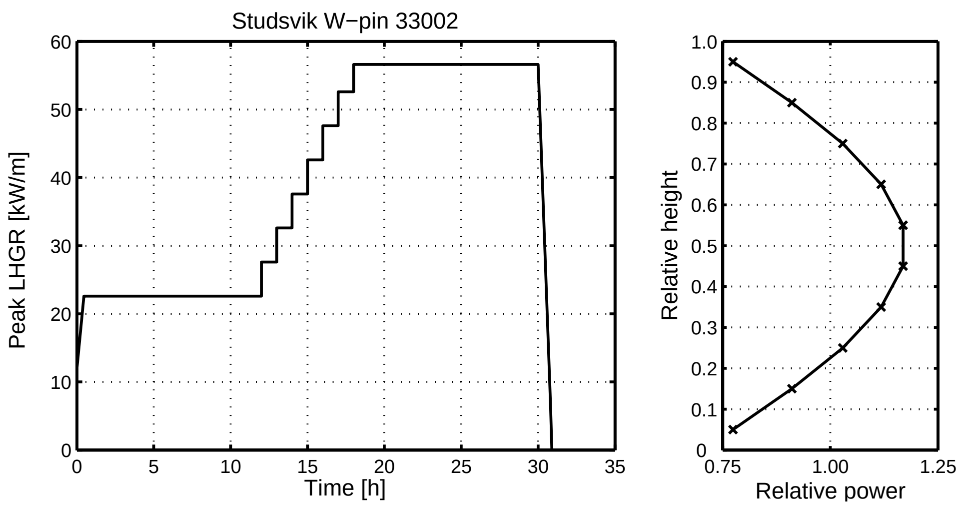

Figure 4. Ramp power history and axial power profile along the fuel column for the Studsvik pin.

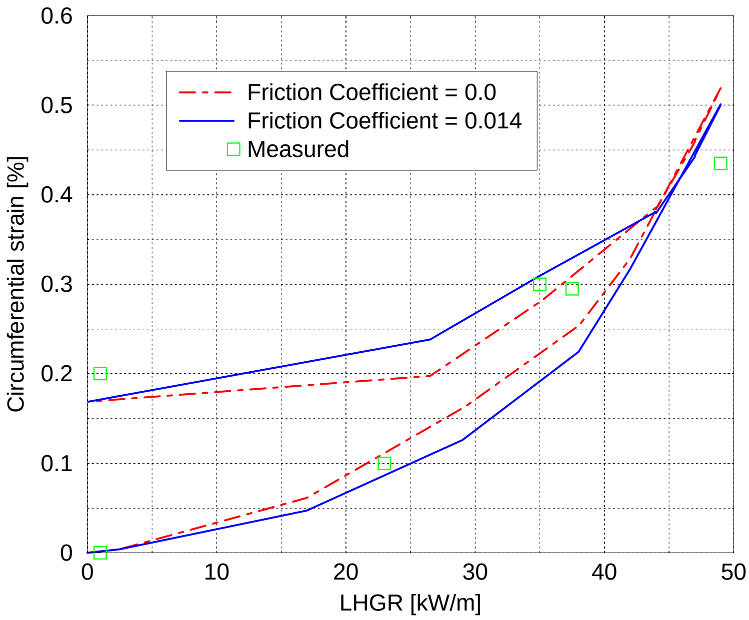

(a)

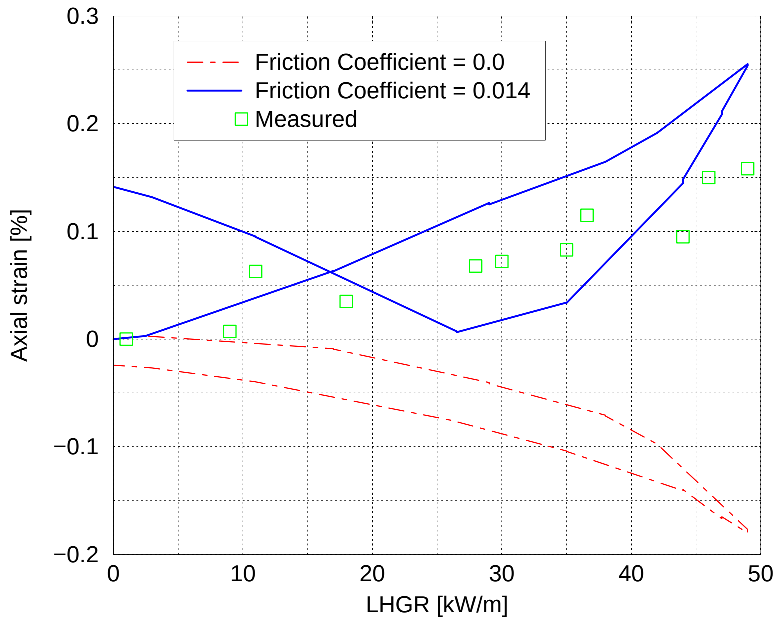

(b)

Figure 5. Comparison between measured and calculated clad strains as a function of linear heat generation rate for the IFA404-1 pin, (a) hoop strain, (b) axial strain.

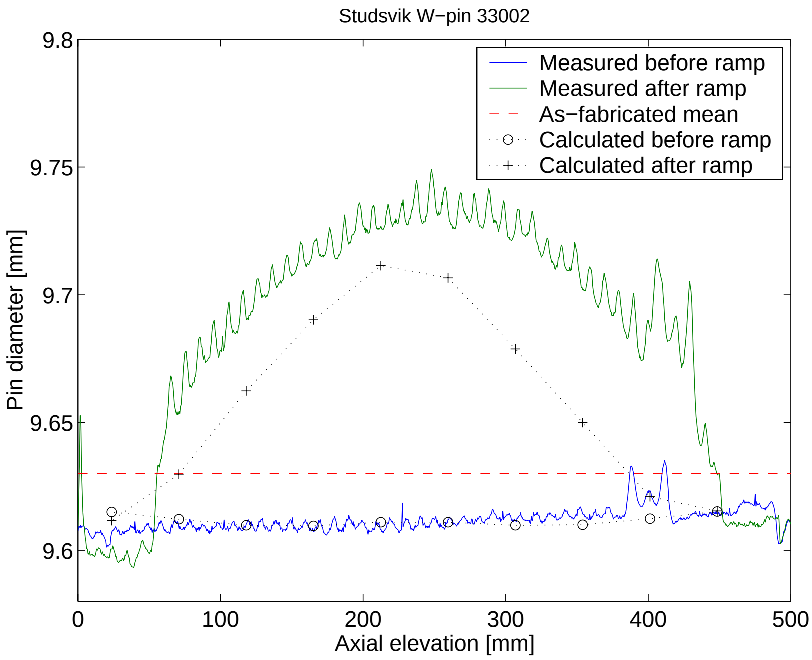

Figure 6. Comparison between measured and calculated clad outer diameter along the pin before and after ramp for the Studsvik pin.

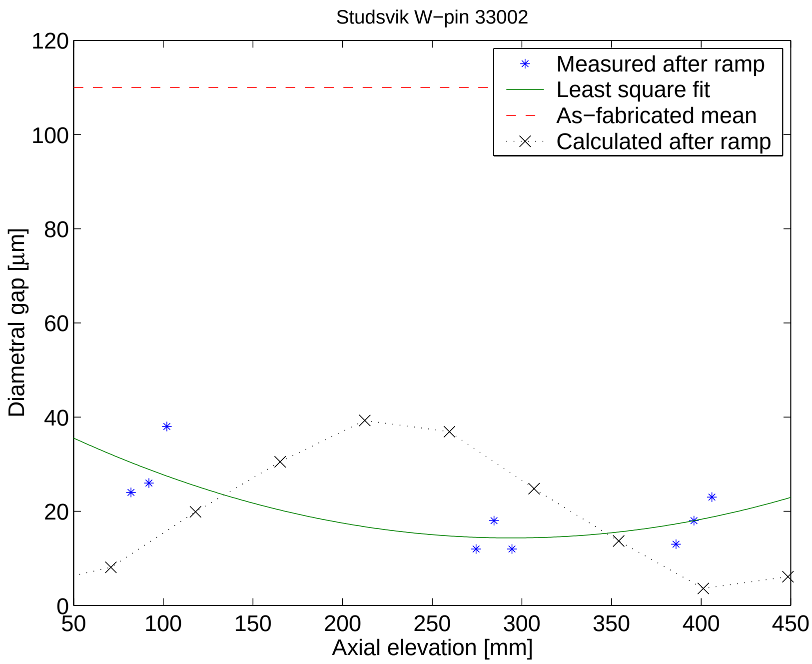

Figure 7. Comparison between measured and calculated pellet-clad gap along the fuel after the ramp for the Studsvik pin. The least square fit line is to the measured data.